BNL-108429-2015-JA

Electronic Structure, Irreversibility Line and Magnetoresistance of $Cu_{0.3}Bi_2Se_3$ Superconductor

Hemian Yi[1], Chaoyu Chen[1], Xuan Sun[1], Zhuojin Xie[1], Ya Feng[1], Aiji Liang[1], Yingying Peng[1], Shaolong He[1], Lin Zhao[1], Guodong Liu[1], Xiaoli Dong[1], Jun Zhang[1], Chuangtian Chen[2], Zuyan Xu [2], Genda Gu[3] and X. J. Zhou[1,4*]

[1] *Beijing National Laboratory for Condensed Matter Physics, Institute of Physics, Chinese Academy of Sciences, Beijing 100190, China*

[2] *Technical Institute of Physics and Chemistry, Chinese Academy of Sciences, Beijing 100190, China.*

[3] *Condensed Matter Physics and Materials Sciences Department, Brookhaven National Laboratory, Upton, New York 11973, USA*

[4] *Collaborative Innovation Center of Quantum Matter, Beijing, China*

[*] *Corresponding author: XJZhou@aphy.iphy.ac.cn.*

(Dated: May 1, 2015)

$Cu_xBi_2Se_3$ is a superconductor that is a potential candidate of topological superconductor. We report our laser-based angle-resolved photoemission measurement on the electronic structure of the $Cu_xBi_2Se_3$ superconductor, and a detailed magneto-resistance measurement in both normal and superconducting states. We found that the topological surface state of the pristine Bi_2Se_3 topological insulator remains robust after the Cu-intercalation but the Dirac cone location moves downward due to electron doping. Detailed measurements on the magnetic field-dependence of the resistance in the superconducting state establishes an irreversibility line and gives a value of the upper critical field at zero temperature of ∼4000 Oe for the $Cu_{0.3}Bi_2Se_3$ superconductor with a middle point T_c of 1.9 K. The relation between the upper critical field H_{c2}(T) and temperature is different from the usual scaling relation found in cuprates and other kinds of superconductors. Small positive magneto-resistance is observed in $Cu_{0.3}Bi_2Se_3$ superconductor up to room temperature. These observations provide useful information for further study of this possible candidate of topological superconductor.

PACS numbers:

Topological insulators are a new quantum state of matter with protected edge or surface states that originates from its unique bulk band topology[1, 2]. Recently, the topological classification of band structures has been extended from spin-orbit-coupled band structures with time-reversal symmetry[3] to other distinct symmetry classes such as crystal point group symmetry[4], magnetic translation symmetry[5] and particle-hole symmetry[6], which leads to new families of topological phases such as topological crystalline insulators[7–10], topological magnetic insulators[11] and topological superconductors[12], respectively. These topological materials not only have potential applications in spintronics and quantum computing[13, 14], but also provide a promising platform for realizing exotic quantum phenomena[15–22] including revelation of Majorana fermions[23, 24], whose antiparticles are themselves, that have attracted great interest in condensed matter physics recently because of their exotic non-Abelian quantum statistics[25]. There are several potential systems which have been proposed to host Majorana fermions[26–29]. Topological superconductors have attracted particular attention because they have a full pairing gap in the bulk and gapless surface states consisting of Majorana fermions[1, 2].

It was discovered that, when a prototypical three-dimensional topological insulator Bi_2Se_3[30, 31] is intercalated with Cu, it can become superconducting in $Cu_xBi_2Se_3$ with the Cu concentration of $0.1 < x < 0.6$ and an optimal critical temperature $T_C \sim 3.8$ K[32–38]. It is thus interesting to investigate whether superconducting $Cu_xBi_2Se_3$[32] can be a topological superconductor[39]. The observation of a zero-bias conductance peak in recent point-contact spectroscopy measurements[35, 38, 40, 41] has supported the possibility of unconventional pairing symmetry in $Cu_xBi_2Se_3$ superconductor and was interpreted as a signature of the topological surface states associated with nontrivial topological superconductivity. On the other hand, the measurement of scanning tunneling spectroscopy (STS) indicates an s-wave pairing symmetry in superconducting $Cu_xBi_2Se_3$[42]. Further work remains to be done to clarify the pairing symmetry and the nature of superconductivity in this material. In this letter, we present our angle-resolved photoemission (ARPES) measurement on the electronic structure of the $Cu_xBi_2Se_3$ superconductor, and a detailed magneto-resistance measurement in both normal and superconducting states. We found that the topological surface state of the pristine Bi_2Se_3 topological insulator remains robust after the Cu-intercalation, although its Dirac point position changes. The temperature-dependence of the magnetoresistance of superconducting $Cu_{0.3}Bi_2Se_3$ gives a value of the upper critical field at zero temperature of ∼4000 Oe for the $Cu_{0.3}Bi_2Se_3$ superconductor with a middle point T_c of 1.9 K. The relation between the H_{c2}(T) and temperature is different from that usually found in cuprates and other kinds of superconductors. We observed small positive magneto-resistance in $Cu_{0.3}Bi_2Se_3$ superconductor up to room temperature. Its small magnitude compared to pristine nanoplate form of Bi_2Se_3 may be due to enhanced electron scattering from large sample inhomogeneity and Cu-intercalation.

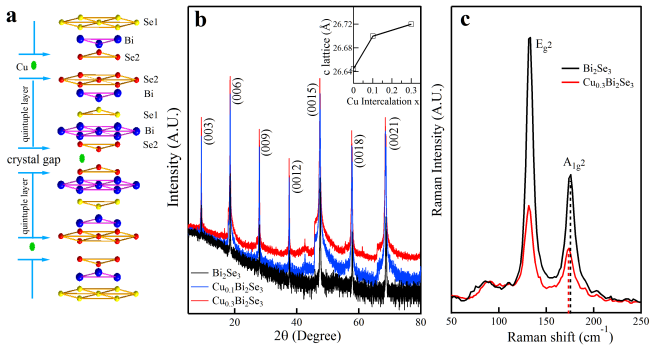

FIG. 1: Crystal structure and characterization of $Cu_xBi_2Se_3$ single crystals. (a). Crystal structure of $Cu_xBi_2Se_3$ showing the quintuple layers and the location of the Van der Waals gaps. (b). X-ray diffraction patterns measured at room temperature on the $Cu_xBi_2Se_3$ (x=0, 0.1 and 0.3) crystal surface that corresponds to the ab plane. The inset plots variation of the c axis lattice constant with x in $Cu_xBi_2Se_3$. (c). Raman spectra of Bi_2Se_3 and $Cu_{0.3}Bi_2Se_3$ measured at room temperature. There are two main Raman-active phonon peaks observed in the measured energy range.

Single crystals of Bi_2Se_3 and $Cu_xBi_2Se_3$ were synthesized by both the melt-growth method and the travelling solvent floating zone method[32, 43, 44]. Single crystal X-ray diffraction (XRD) patterns of $Cu_xBi_2Se_3$ samples were examined at room temperature by use of a rotating anode X-ray diffractometer with Cu K_α radiation (λ = 1.5418 $\AA$). Raman scattering spectra were collected at room temperature by use of a JY HR800 Raman spectrometer with $\lambda = 532$ nm laser. The standard four-probe technique was used for resistance measurements with the electric current flowing in the basal plane of the crystals and the magnetic field applied perpendicular to the basal plane. The measurement was performed by using a Quantum Design physical properties measurement system (PPMS). The magnetic susceptibility was measured by using a superconducting quantum-interference device magnetometer (SQUID-MPMS). The ARPES measurements were performed on our Lab photoemission system equipped with the Scienta R4000 electron energy analyzer[44, 45]. A vacuum ultra-violet (VUV) laser with a photon energy of 6.994 eV[45] was used as the light source. The overall energy resolution used in this case is 1.5 meV and the angular resolution is ~0.3 degree. The Fermi level is referenced by measuring the Fermi edge of a clean polycrystalline gold that is electrically connected to the sample. The crystals were cleaved *in situ* and measured at a temperature of T~20 K in vacuum with a base pressure better than 5×10^{-11}Torr .

Figure 1a shows the crystal structure of Cu-intercalated Bi_2Se_3 which has a layered structure with a triangle lattice within one layer. The material consists of five-atomic-layer unit arranged as the Se2-Bi-Se1-Bi-Se2 sequence along the c-direction known as quintuple layers, as indicated in Fig. 1a. The coupling within the quintuple layers is strong but becomes much weaker, predominantly of the van der Waals type gap, between two quintuple layers. The intercalated Cu can enter through the van der Waals gap. Fig. 1b displays the XRD patterns on the surface of $Cu_xBi_2Se_3$ (x=0, 0.1 and 0.3) single crystals. The observed peaks can be well indexed to (0 0 3n) reflections which agree with the R-3m space group of Bi_2Se_3. The lattice constant c is calculated and plotted in the inset of Fig. 1b. With the increasing x in $Cu_xBi_2Se_3$, the lattice constant c increases from 28.645 $\AA$ for Bi_2Se_3 to 28.720 for $Cu_{0.3}Bi_2Se_3$. It is likely that the Cu-intercalation into the two adjacent quintuple layers expands the lattice in c direction, consistent with the previous report[46]. Two Raman active phonon modes can be observed in the covered energy range in Fig. 1c. In pure Bi_2Se_3, the peaks at 131.5 cm^{-1} and 175.5 cm^{-1} can be assigned to the E_g^2 mode and A_{1g}^2 mode, respectively[47]. With Cu-intercalation, both of these two peaks shift to lower energy, with an obvious shift for the A_{1g}^2 mode. Since the A_{1g}^2 mode corresponds to atom vibrations along the c direction, the Cu-intercalation will weaken the interactions between the quintuple layers, thus giving rise to the decrease of the mode energy[46].

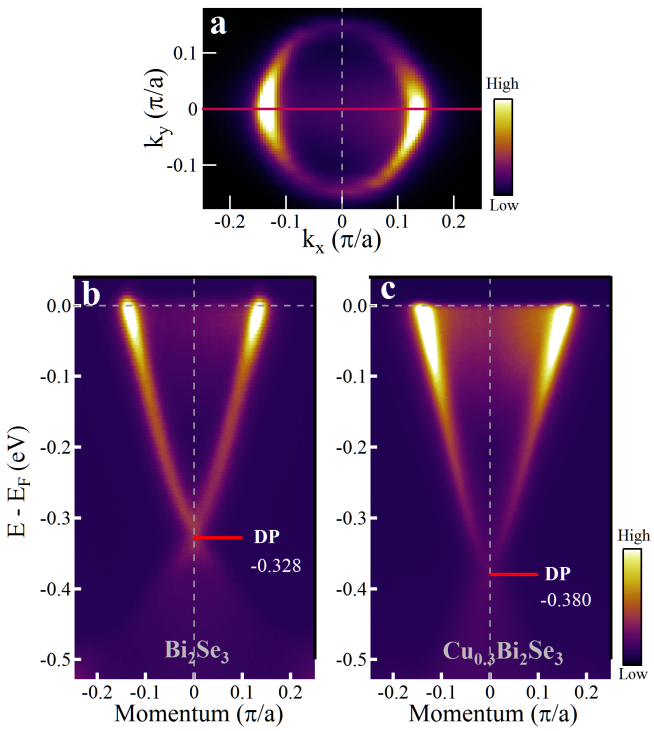

FIG. 2: Topological surface state of Bi_2Se_3 and $Cu_{0.3}Bi_2Se_3$ measured by laser-based ARPES at 20 K. (a). Fermi surface of the topological surface state of Bi_2Se_3. (b). Band structure of the topological surface state of Bi_2Se_3 along the horizonal $\bar{\Gamma}$-$\bar{M}$ direction as shown by the red line in (a). (c). Band structure of the topological surface state of $Cu_{0.3}Bi_2Se_3$ along the same $\bar{\Gamma}$-$\bar{M}$ cut.

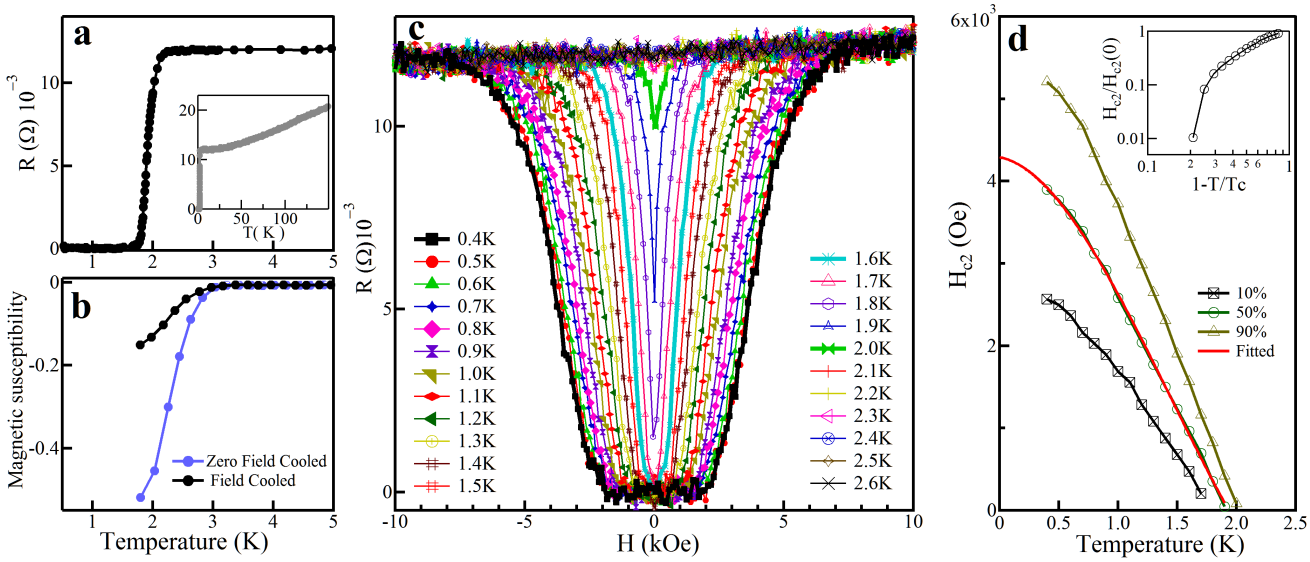

FIG. 3: Transport and magnetic properties of $Cu_{0.3}Bi_2Se_3$. (a). Temperature dependence of resistance of $Cu_{0.3}Bi_2Se_3$ at zero magnetic field. The inset shows the resistance measured over wide temperature range. (b). Temperature dependence of magnetic susceptibility of $Cu_{0.3}Bi_2Se_3$. The magnetic field used is 1 Oe. Blue line is zero-field-cooled curve while the black line is field-cooled curve. Note that the measurements of (a) and (b) were from two different pieces of the $Cu_{0.3}Bi_2Se_3$ samples. Different T_c comes from sample inhomogeneity. (c). Magnetic field dependence of resistance of $Cu_{0.3}Bi_2Se_3$ at various temperatures. (d). Critical field H_{c2} determined at different temperatures using the criterion of 10%, 50% and 90% drop of normal state resistance. The red line represents a WHH fitting of the measured 50% drop result. The upper-right inset shows the relation between the normalized $H_{c2}/H_{c2}(0)$ and $(1\text{-}T/T_c)$ in a logarithmic scale.

Figure 2 compares the electronic structure of Bi_2Se_3 and $Cu_{0.3}Bi_2Se_3$ measured at a temperature of 20 K by our VUV laser-based ARPES. Fig. 2a shows the Fermi surface of the topological surface state in Bi_2Se_3. Figs. 2b and 2c show the band structure measured along the horizontal $\bar{\Gamma}$-$\bar{M}$ momentum cut (red line in Fig. 2a) for Bi_2Se_3 and $Cu_{0.3}Bi_2Se_3$, respectively. The topological Dirac cone structure is well protected in the Cu-intercalated $Cu_{0.3}Bi_2Se_3$ superconductor (Fig. 2c), consistent with the previous report[33]. But the Cu-intercalation into Bi_2Se_3 results in the shift of the Dirac point (DP), from -0.328 eV for the pure Bi_2Se_3 (Fig. 2b) to -0.380 eV for $Cu_{0.3}Bi_2Se_3$ (Fig. 2c). This indicates the Cu-intercalation causes electron-doping into the $Cu_xBi_2Se_3$ system. The clear observation of topological surface state in our laser-ARPES measurements paves a way for the superconducting gap measurements in the near future when the sample can be cooled into the superconducting state.

Figure 3 shows transport and magnetic measurement results of $Cu_{0.3}Bi_2Se_3$. The resistance shows a metallic behavior below 150 K and becomes superconducting with an onset temperature of 2.2 K, midpoint temperature of ∼1.9 K, and a zero resistance temperature of 1.7 K (Fig. 3a). Magnetization measurement on another piece of $Cu_{0.3}Bi_2Se_3$ sample (Fig. 3b) shows a superconducting transition at ∼3 K for both field-cooled and zero-field-cooled measurement modes. The magnetization signal is strong enough to indicate that the measured signal originates from the bulk superconductivity of the sample. We note that different T_c may come from the inhomogeneity that is usually found in Cu-intercalated Bi_2Se_3 samples.

Figure 3c shows detailed magnetic field dependence of the resistance for the superconducting $Cu_{0.3}Bi_2Se_3$ sample measured at different temperatures, giving an overall R(H,T) curves. Taking the resistance curve at 0.4 K for an example (black curve in Fig. 3c), the resistance keeps at zero at low magnetic field (below ∼1700 Oe), then it increases with the increasing magnetic field, and gets saturated near ±8000 Oe. This is a typical resistive behavior of a superconductor under a magnetic field; when the magnetic field exceeds the upper critical field H_{c2}, the sample recovers to its normal state. With increasing temperature, the central zero resistance region gets narrower, and the rising curves on both plus and negative side moves closer to the central line. Around 1.6 K, the central zero resistance region becomes nearly a point. Around 2.2 K, the resistance basically recovers to its normal state at all magnetic field. Fig. 3d shows the upper critical field H_{c2} determined at different temperatures using the criterion of 10%, 50% and 90% drop of the normal state resistance. In superconductors like high T_c cuprates, H_{c2} is usually taken to be at the temperature where R(T,H) drops to 50% of its extrapolated normal-state value[48]. The 50% data in Fig. 3d is fitted by the Werthamer-Helfand-Hohenberg (WHH) formalism[49]. The upper critical field at zero temperature obtained is 4284Oe. It is interesting to note that,

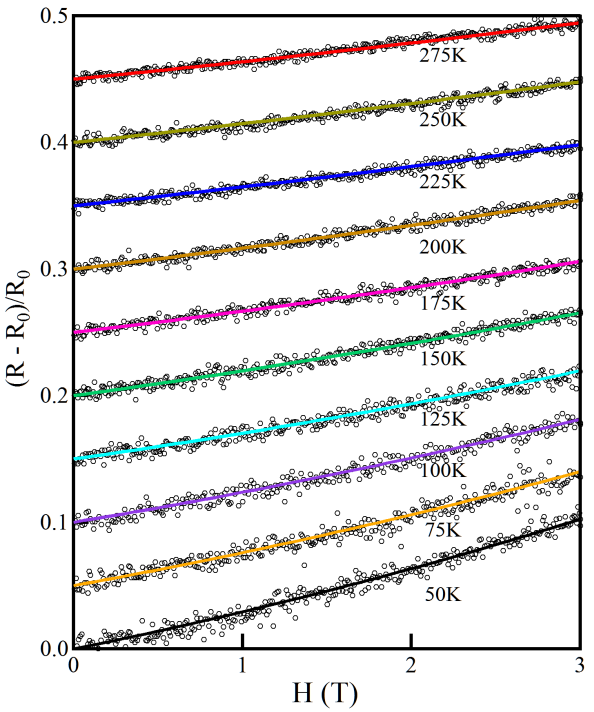

FIG. 4: Normal state magnetoresistance of $Cu_{0.3}Bi_2Se_3$ superconductor. Variation of resistance of $Cu_{0.3}Bi_2Se_3$ as a function of magnetic field measured at different temperatures. The measured data (black empty circles) are fitted by using a function with a linear term and a 2nd order term. For clarity, the curves are offset 0.05 sequentially along the vertical axis.

for $Cu_xBi_2Se_3$ with a midpoint critical temperature of 3.2 K, the measured upper critical field reaches 30000 Oe[35]. In comparison, the zero-temperature H_{c2} value (4284 Oe) of our $Cu_xBi_2Se_3$ sample with a midpoint Tc∼1.9 K is much reduced.

It is now well-established that both high T_c and low T_c superconductors may exhibit a vortex solid to liquid phase transition[48, 50–52] where the transition line can be fitted by a relation $H \sim (1 - T^*/T_c)^n$ with n being a characteristic exponent. In (Ba,K)BiO_3 superconductor, such a scaling is observed for the entire curve[52]. In high-T_c cuprates, the irreversibility line H(T^*) obeys a scaling relationship with n = 3/2 near T_c with a crossover to a more rapid temperature dependence below about T/T_c =0.6[48]. It is interesting to examine whether such a scaling behavior is present in $Cu_xBi_2Se_3$ superconductor. Fig. 3d inset shows the irreversibility line relationship of $Cu_{0.3}Bi_2Se_3$ determined by midpoint resistance. It shows nearly a linear relation with 1-T/T_c between 0.4 and 1 followed by a rapid decrease when 1-T/T_c is below 0.4. Such a behavior is obviously different from the high-T_c cuprates[48]. More work needs to be done to understand the flux behavior in $Cu_xBi_2Se_3$ superconductor.

It has been found that the nanoplate form of Bi_2Se_3 exhibits large magnetoresistance at low temperature (up to 400%) and room temperature (up to 75%)[53]. Here we study the magnetoresistive behavior of $Cu_xBi_2Se_3$ superconductor in its normal state. Fig. 4 shows the magnetic field dependence of the resistance of $Cu_{0.3}Bi_2Se_3$ at different temperatures up to room temperature. The magnetic field is applied perpendicular to the basal ab plane. As seen in Fig. 4, the resistance increases with increasing magnetic field indicating a positive magneto-resistive behavior. Also, the magneto-resistive behavior gets weaker with increasing temperature. However, the overall magnitude of magnetoresistance of $Cu_xBi_2Se_3$ is much smaller than that in nano-plate Bi_2Se_3. It has been found that the magnetoresistance is closely related to electron mobility[53]. The smaller magneto-resistance in $Cu_xBi_2Se_3$ can be due to enhanced electron scattering from impurities and disorder introduced by both the large sample volume (compared with the nanoplate) and the Cu intercalation.

In summary, we have presented investigations of structural characterization, electronic structure and magneto-transport properties of the Cu-intercalated $Cu_xBi_2Se_3$ superconductor. Our laser-ARPES study indicated that, upon Cu-intercalation, the topological surface states are robust in $Cu_xBi_2Se_3$ but the Dirac cone location is altered due to electron doping. This lays a foundation for further study on the superconducting gap symmetry by ARPES when it is possible to cool down the sample in the superconducting state. Our detailed measurements on the magnetic field-dependent superconducting transition at different temperatures establish an irreversibility line and give a value of the upper critical field at zero temperature of ∼4000 Oe for the $Cu_{0.3}Bi_2Se_3$ superconductor with a mid-point T_c of 1.9 K. The relation between the H_{c2}(T) and temperature is different from the scaling relationship usually found in cuprates and other kinds of superconductors. We observed small positive magneto-resistance in $Cu_{0.3}Bi_2Se_3$ superconductor up to room temperature. Its small magnitude compared to pristine nanoplate form of Bi_2Se_3 may be due to enhanced electron scattering from large sample inhomogeneity and Cu-intercalation. These observations provide useful information for further study of this possible candidate of topological superconductor.

Acknowledgement We thank Yingzi Zhang for useful discussions. This work is supported by the National Natural Science Foundation of China (11190022, 91021006 and 11374338), the MOST of China (973 program No: 2011CB921703, 2011CBA00110 and 2013CB921700), and the Strategic Priority Research Program (B) of the Chinese Academy of Sciences (Grant No. XDB07020300).

[1] M. Z. Hasan and C. L. Kane, Rev. Mod. Phys. **82**, 3045 (2010).
[2] X. L. Qi and S. C. Zhang, Rev. Mod. Phys. **83**, 1057 (2011).
[3] J. E. Moore, Nature **464**, 194 (2010).
[4] L. Fu, Phys. Rev. Lett. **106**, 106802 (2011).
[5] R. S. K. Mong et al., Phys. Rev. B **81**, 245209 (2010).
[6] A. P. Schnyder et al., Phys. Rev. B **78**, 195125 (2008).
[7] T. H. Hsieh et al., Nat. Commun. **3**, 982 (2012).
[8] Y. Tanaka et al., Nat. Phys. **8**, 800 (2012).
[9] S. Y. Xu et al., Nat. Commun. **3**, 1192 (2012).
[10] P. Dziawa et al., Nat. Mater. **11**, 1023 (2012).
[11] J. Wang et al., Phys. Rev. Lett. **106**, 126403 (2011).
[12] X. L. Qi, et al., Phys. Rev. Lett. **102**, 187001 (2009).
[13] X. L. Qi and S. C. Zhang, Phys. Today **63**, 33 (2010).
[14] J. Moore, Nat. Phys. **5**, 378 (2009).
[15] B. A. Bernevig et al., Science **314**, 1757 (2006).
[16] M. Konig et al., Science **318**, 766 (2007).
[17] H. J. Zhang et al., Phys. Rev. Lett. **111**, 066801 (2013).
[18] Z. J. Xie et al., Nat. Commun. **5**, 3382 (2014).
[19] X. L. Qi et al., Science **323**, 1184 (2009).
[20] R. Yu et al., Science **329**, 61 (2010).
[21] C. Z. Chang et al., Science **340**, 167 (2013)
[22] R. Li et al., Nat. Phys. **6**, 284 (2010).
[23] E. Majorana, Nuovo Cimento **14**, 171(1937).
[24] F. Wilczek, Nat. Phys. **5**, 614 (2009).
[25] G. Moore and N. Read, Nucl. Phys. B **360**, 362 (1991).
[26] N. Read and D. Green, Phys. Rev. B **61**, 10267 (2000).
[27] S. Das Sarma et al., Phys. Rev. B **73**, 220502 (2006).
[28] L. Fu and C. L. Kane, Phys. Rev. Lett. **100**, 096407 (2008).
[29] L. Fu and C. L. Kane, Phys. Rev. Lett. **102**, 216403 (2009).
[30] H. J. Zhang et al., Nat. Phys. **5**, 438 (2009).
[31] Y. Xia et al., Nat. Phys. **5**, 398 (2009).
[32] Y. S. Hor et al., Phys. Rev. Lett. **104**, 057001 (2010).
[33] L. A. Wray et al., Nat. Phys. **6**, 855 (2010).
[34] P. Das et al., Phys. Rev. B **83**, 220513 (2011).
[35] S. Sasaki et al., Phys. Rev. Lett. **107**, 217001 (2011).
[36] M. Kriener et al., Phys. Rev. B **84**, 054513 (2011).
[37] M. Kriener et al., Phys. Rev. Lett **106**, 127004 (2011).
[38] S. Sasaki et al., Phys. Rev. Lett **109**, 217004 (2012).
[39] L. Fu and E. Berg, Phys. Rev. Lett. **105**, 097001 (2010); L. Fu, Phys. Rev. B **90**, 100509 (2014).
[40] T. Kirzhner et al., Phys. Rev. B **86**, 064517 (2012).
[41] X. Chen et al., arXiv:1210.6054.
[42] N. Levy et al., Phys. Rev. Lett. **110**, 117001 (2013).
[43] J. A. Schneeloch et al., Phys. Rev. B **91**, 144506 (2015).
[44] C. Y. Chen et al., PNAS **109**, 3694 (2012).
[45] G. Liu et al., Rev. Sci. Instrum. **79**, 023105 (2008).
[46] H. J. Chen et al., Appl. Phys. Lett. **101**, 121912 (2012).
[47] Y. Kim et al., App. Phys. Lett. **100**, 071907 (2012).
[48] C. C. Almasan et al., Phys. Rev. Lett. **69**, 3812 (1992).
[49] N. R. Werthamer, E. Helfand, P. C. Hohenberg, Phys. Rev. **147**, 295 (1966).
[50] M. Suenaga et al., Phys. Rev. Lett. **66**, 1777 (1991).
[51] M. F. Schmidt et al., Phys. Rev. Lett. **70**, 2162 (1993).
[52] T. Klein et al., Phys. Rev. B **58**, 12411 (1998).
[53] Y. Yan et al., App. Phys. Lett. **103**, 033106 (2013).